Electronic Supplementary Material (ESI) for Sustainable Energy & Fuels.

A synergistic construction of iron nitride embedded graphitic carbon nitride heterostructure electrocatalyst as potential candidate to accelerate overall water electrolysis.

Venkatachalam Ashok, Arunagiri Gayathri, Murugan Vijayarangan and Jayaraman Jayabharathi*

Department of chemistry, Material Science Lab, Annamalai University, Annamalai Nagar, Tamilnadu-608 002, India.

E-mail: jtchalam2005@yahoo.co.in

Materials

Potassium ferrocyanide ($K_4[Fe(CN)_6].3H_2O$) and received from SISCO CHEM, potassium hydroxide (KOH) was received form Nice Chemical Pvt. Ltd. Hydrochloric acid and acetone purchased from SD Fine chemical Ltd. Nickel Foam (NF) received from Vitra Technologies, India. Iridium Oxide (IrO_2), Platinum derived carbon (Pt-C) and Nafion 15% received from Sigma Aldrich. All chemicals used as received without any further purification. The deionized water was used thought the experiment.

Physical characterization

High resolution transmission electron microscopy (HR-TEM) conducted on a JEOL JEM 2200FS microscope operated at 200 kV acceleration voltage, probe-side C_s-corrected, integrated with an Oxford X Max 100 Energy Dispersive X-ray (EDX) detector. Field Emission Scanning Electron Microscopy (FE-SEM) was conducted on ZEISS oxford and an accelerated voltage at 3 kV with the measurement of EDX. Structural interpretation of Fe_3N@CN-x identified with x-ray diffraction (XRD), were taken on a powder diffractrometer (Rigaku, D/MAX, 2500 V) with Cu Kα radiation (λ=1.54056 Å) operating at 40 KV and 250 mA. Raman shift were measured by using Raman spectroscopy (Renishaw) with a 514.5 nm laser excitation. Chemical bond structure identified based on Fourier Transform Infrared (FT-IR) spectrometer ThermoNicolet 6700. XPS measurements were carried out in an ultra-high vacuum (UHV) set-up equipped with a monochromatic Al KαX-ray source (1486.6 eV; anode operating at 12.25 kV and 300 W) and a high resolution Phoibos 150 MCD analyzer (SPECS). Thermogravimetric and differential thermal analysis (TG-DTA) was analyzed NETZSCH STA 449F3 instrument with alumina crucible in N_2 atmosphere temperature rate at 10 K/min. X-ray photoemission spectra were measured in fixed analyzer transmission mode with pass energy 20 eV and step size 0.5 and 0.05 eV for survey and

region scans correspondingly. The surface area and pore size characteristics of synthesized samples were analyzed by N_2 adsorption and desorption measurements using a Micromeritics (Tristar11) surface area and porosity analyzer. Samples were degassed at a temperature of 200 °C before the adsorption measurements.

Electrochemical measurement

The electrochemical measurement was carried out in a Biologic-SP200 workstation. In the electrochemical cell, conventional three electrode configuration consist of the as prepared catalyst loaded onto nickel foam used as a working electrode, saturated calomel electrode (SCE) and graphite rod served as reference and counter electrodes, respectively. Prior to electrochemical measurement NF was cleaned with 0.1 M HCl solution and acetone dried in oven. All electrochemical analysis are carried out in 1.0 M KOH solution and data was reported without iR-drop correction. The polarization curves were obtained by linear sweep voltammetry (LSV) with scan rate of 5 mV/s and stability measurement analyzed with chronopotentiometry at 10 mA/cm^2. From the linear sweep voltammetry (LSV) plots, the Tafel plots were derived by plotting as overpotential versus log of current density. Subsequently, Tafel slopes can be determined by fitting the linear parts of Tafel plots using Tafel equation of $\eta = a + b \log (j)$, where, η, a, b and j indicates the overpotential, Tafel constant, Tafel slope and current density, correspondingly. Electrochemical impedance spectrum was taken in the range of 100 KHz to 10 mHz with applied potential 0.5 V *vs*. RHE.

The conventional potential conversion, SCE to RHE is as follows [1].

$$E_{RHE}=E_{SCE} + 0.0591\ pH + 0.242$$

Overall water splitting was conducted in a two-electrode system. In the experiment Fe_3N@CN/NF employed as a both anode and cathode and comparison analysis precious couple of Pt-C/NF||IrO_2/NF are evaluated in 1.0 M KOH with scan rate of 10 mV/s.

Fe_3N@CN-x, Pt-C, and IrO_2 catalyst ink preparation

About 2 mg of each catalyst was ultrasonically dispersed in a mixture of 1 mL water 20µm Nafion. Finally the ink was loaded on nickel foam (0.5 mg/cm^2) and dried under 60°C in oven.

Turnover frequency

Turnover frequency were calculated with the following equation: TOF = j x A/z x n x F, where, j- current density, A-actual electrode surface area, z- number of electrons (for OER, n=4 and HER, n=2), m- mass of the catalyst loading and F- faraday constant (96485 C mol^{-1}) [2].

Calculation of O_2/H_2 generation

Based on the displaced amount of water due to the O_2/H_2 bubbles, the amount of O_2/H_2 generated was calculated using the following equations

Amount of O_2/H_2 generated in 1 h = amount of water displaced in liters (1)

$$\left.\begin{array}{l}\text{Amount of } O_2/H_2 \text{ generated in} \\ \text{moles for 1 h}\end{array}\right\} = \frac{\text{amount of water displaced (liters)}}{22.4 \text{ liters}} \quad (2)$$

We have also calculated the O_2/H_2 generation rate from the electrical charge passed through the electrode using the equation given below.

$$\left(\begin{array}{l}\text{Current obtained} \\ \text{During water electrolysis}\end{array} \quad X \quad \begin{array}{l}\text{Time duration for} \\ \text{each potential}\end{array}\right) = \text{Coulomb} \quad (3)$$

$$\frac{\text{Coulomb x F}}{96485C} = \text{No. of moles of } e^- \text{ for } O_2/H_2 \text{ generation} \quad (4)$$

$$\frac{\text{No. of moles of } e^- \text{ for } O_2/H_2 \text{ generation x 1 mole of } O_2/H_2 \text{ gas}}{4/2 \text{ moles of electron}} = \text{Moles of } O_2/H_2 \text{ generated} \quad (5)$$

Faradaic Efficiency

At constant potential of 1.64 V given across the Fe_3N@CN-700/NF||Fe_3N@CN-700/NF electrode couples assembled and sealed in H-type full cell in 1.0 M KOH. During the electrolysis, evolved gas molecules were measured by water displacement method. The applied potential can provide 10 mA/cm^2 current density to the system and the electrolysis was monitored 60 min. each 10 min of analysis data shown in the data (Figure S10). Theoretical number of moles of gas molecules can be calculated from Faraday's second law of electrolysis according to the following equation [3].

$$V_t = Q/nF$$

where, V_t is the number of oxygen and hydrogen molecules calculated theoretically, Q-total charge passed to the cell systems, n-number of electrons (n=4 for O_2 and n=2 for H_2) and F-Faraday constant 96485.3 C/mol.

The Faradaic Efficiency of OER/HER was estimated using the following equation:

$$FE = 4Fn_{O2}/It \times 100\%$$

$$FE = 2Fn_{H2}/It \times 100\%$$

Where, F is Faraday constant (96485 C/mol), n_{O2} is the number of moles of experimental O_2 during the reaction (mol), n_{H2} is the number of moles of experimental H_2 during the reaction (mol), I is the current of the reaction (A), and t is the reaction time (s) [4].

Figure S1. XRD spectra of potassium ferrocyanide and as-prepared Fe_3N@CN-700

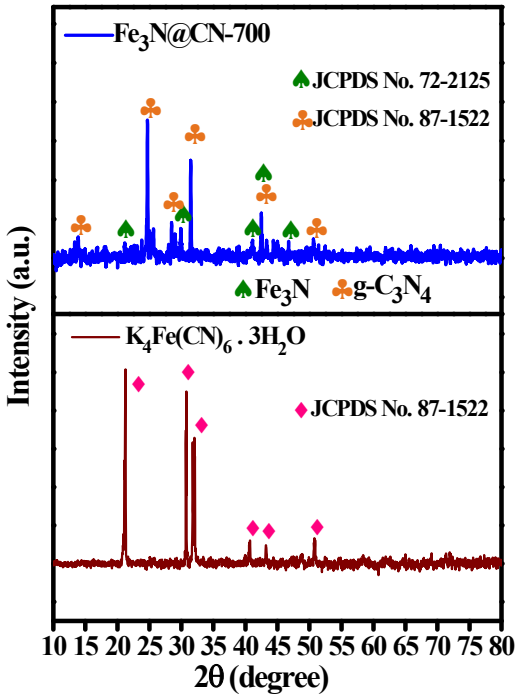

Figure S2. Comparison FT-IR spectra of potassium ferrocyanide with Fe_3N@CN-700 electrocatalyst.

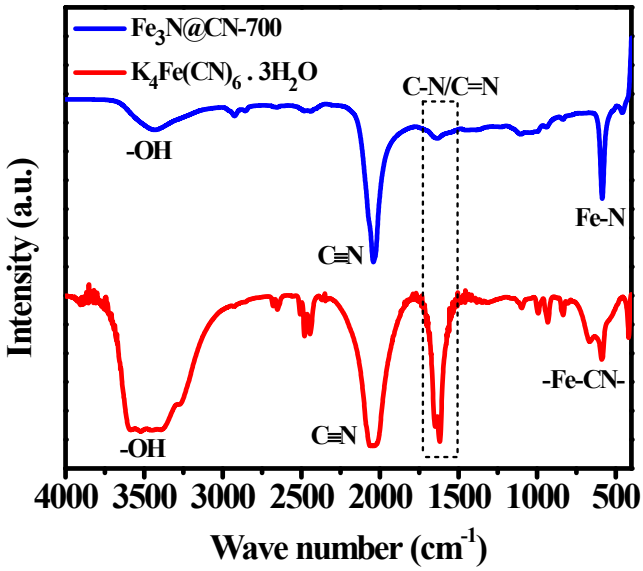

Figure S3. TG-DTA analysis of potassium ferrocyanide.

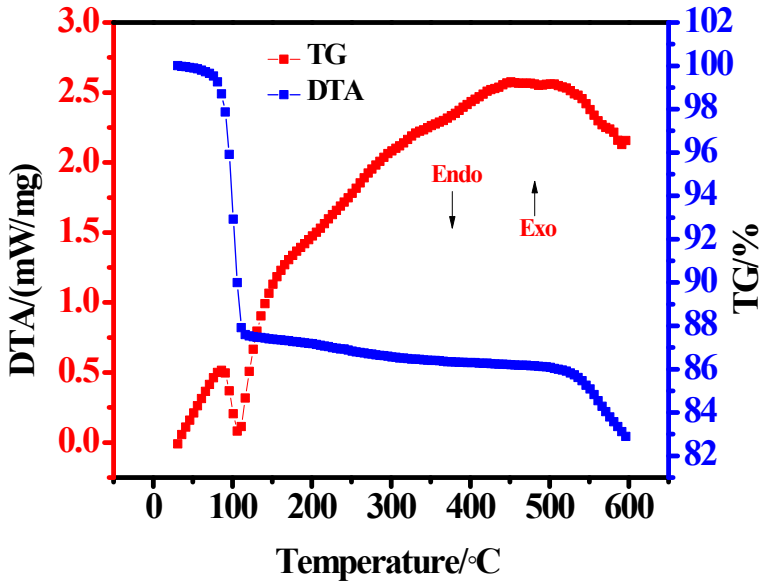

Figure S4. HR-TEM images of Fe_3N@CN-800 (a) and (b).

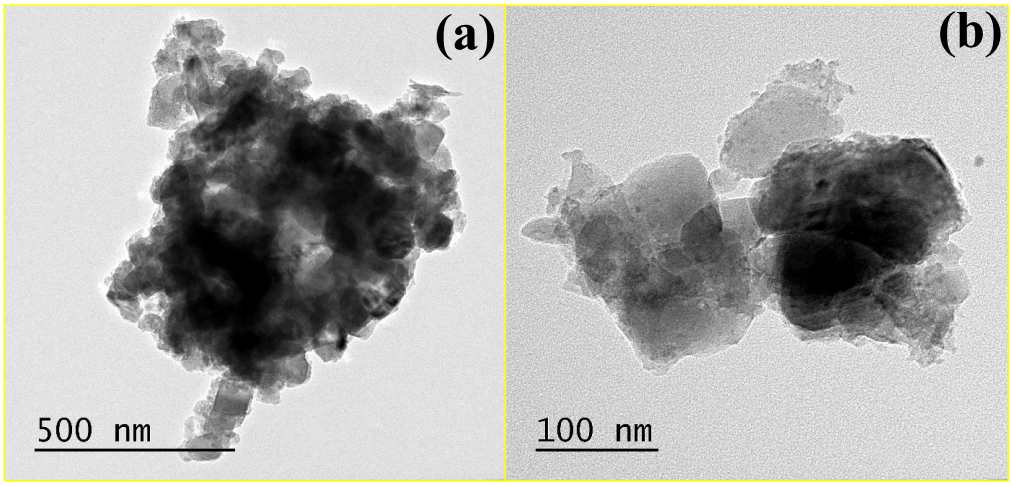

Figure S5. Raman spectra of variously pyrolyzed Fe_3N@CN-x electrocatalyst.

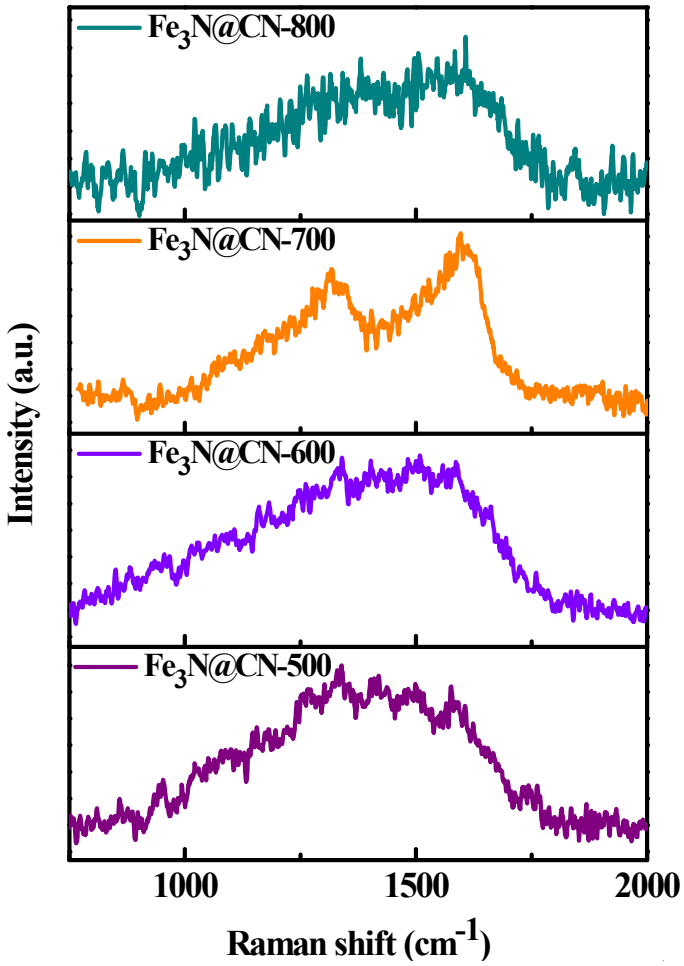

Figure S6. N_2 adsorption-desorption isotherm (a) and BJH pore size distribution (b) of Fe_3N@CN-x

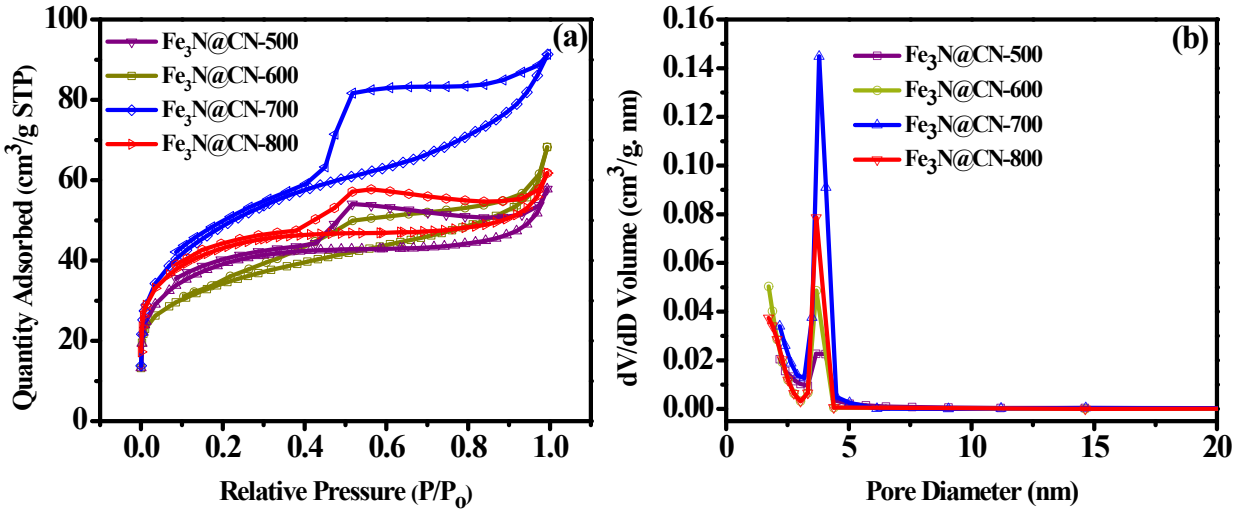

Figure S7. XPS oxygen spectrum of Fe_3N@CN-700

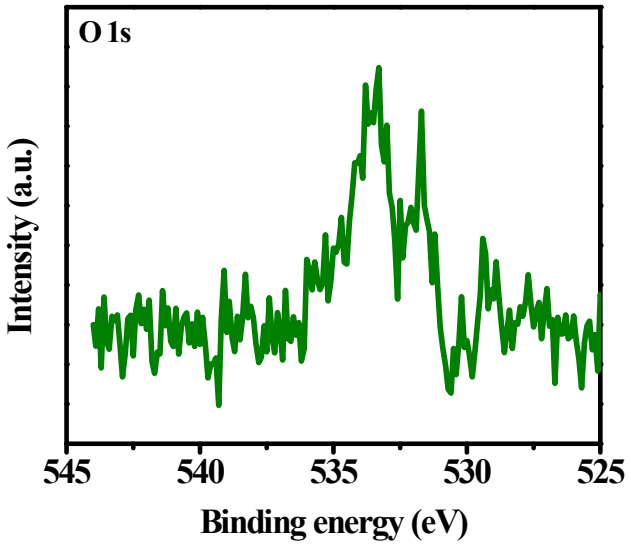

Figure S8. XPS spectra of potassium ferrocyanide Fe 2p (a), O 1s (b), N 1s (c) and K 2p with C1s (d).

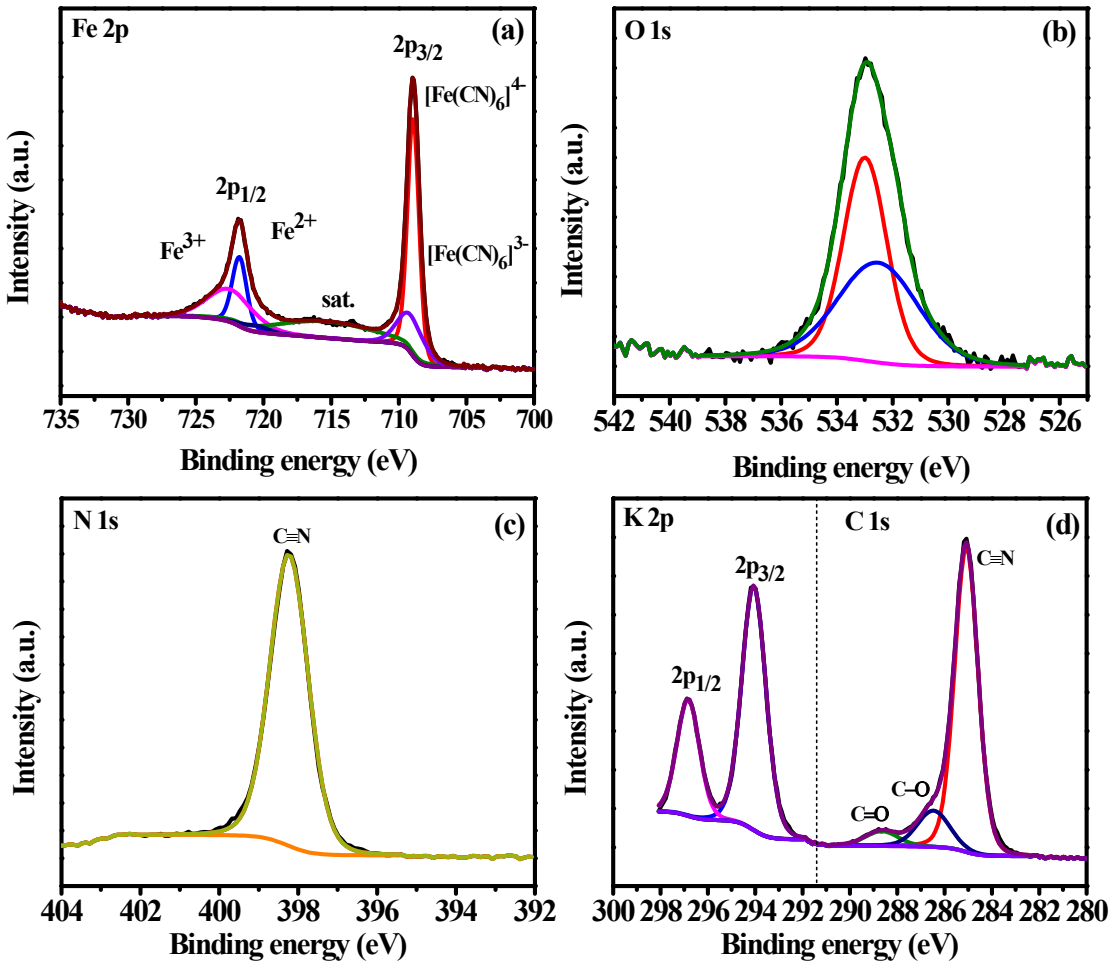

From the XPS spectra of potassium ferrocyanide the Fe 2p shows five deconvoluted peaks. At first, the main peak of $2p_{3/2}$ has been deconvoluted into three peaks at 708.2 eV, 709.8 eV and 714.8 eV attributed to $[Fe(CN)_6]^{4-}$, $[Fe(CN)_6]^{3-}$ and Fe^{3+} peak, respectively (Figure S7a) [5] whereas the another main peak of $2p_{3/2}$ can be deconvoluted to two peaks positioned at 721.8 eV and 722.6 eV assigned to Fe^{2+} and Fe^{3+}, respectively [6]. The O 1s spectrum contained two deconvoluted peaks at 532.4 eV and 532.9 eV, which can be related to the structurally bonded H_2O and pre-existed water molecules, respectively (Figure S7b) [7]. The N 1s spectrum shows a dominant main peak at 398.5 eV related to the nitrogen in cyanide ligand (Figure S7c) [8]. The Figure S7d shows the C 1s

with K 2p spectra, the carbon binding energy with 285.0 eV is carbon from the cyanide group while the other two peaks of 285.8 eV and 288.8 eV corresponding to the C-O and C=O respectively, due to some degree of stoichiometric contaminant present on sample surfaces [7]. The K 2p spectrum has two main peaks of $2p_{3/2}$ and $2p_{1/2}$ which also ascertain the existence of potassium in the precursor material [7]. The overall binding energy of individual elements of Fe, C, N, O and K were utterly deviated and some peaks like oxygen and potassium were completely vanished after the pyrolysis treatment which confirmed the synergistic construction of iron nitride embedded graphitic carbon nitride electrocatalyst.

Figure S9. Electrochemical active surface area CV's of Fe_3N@CN-x in 1.0 M KOH.

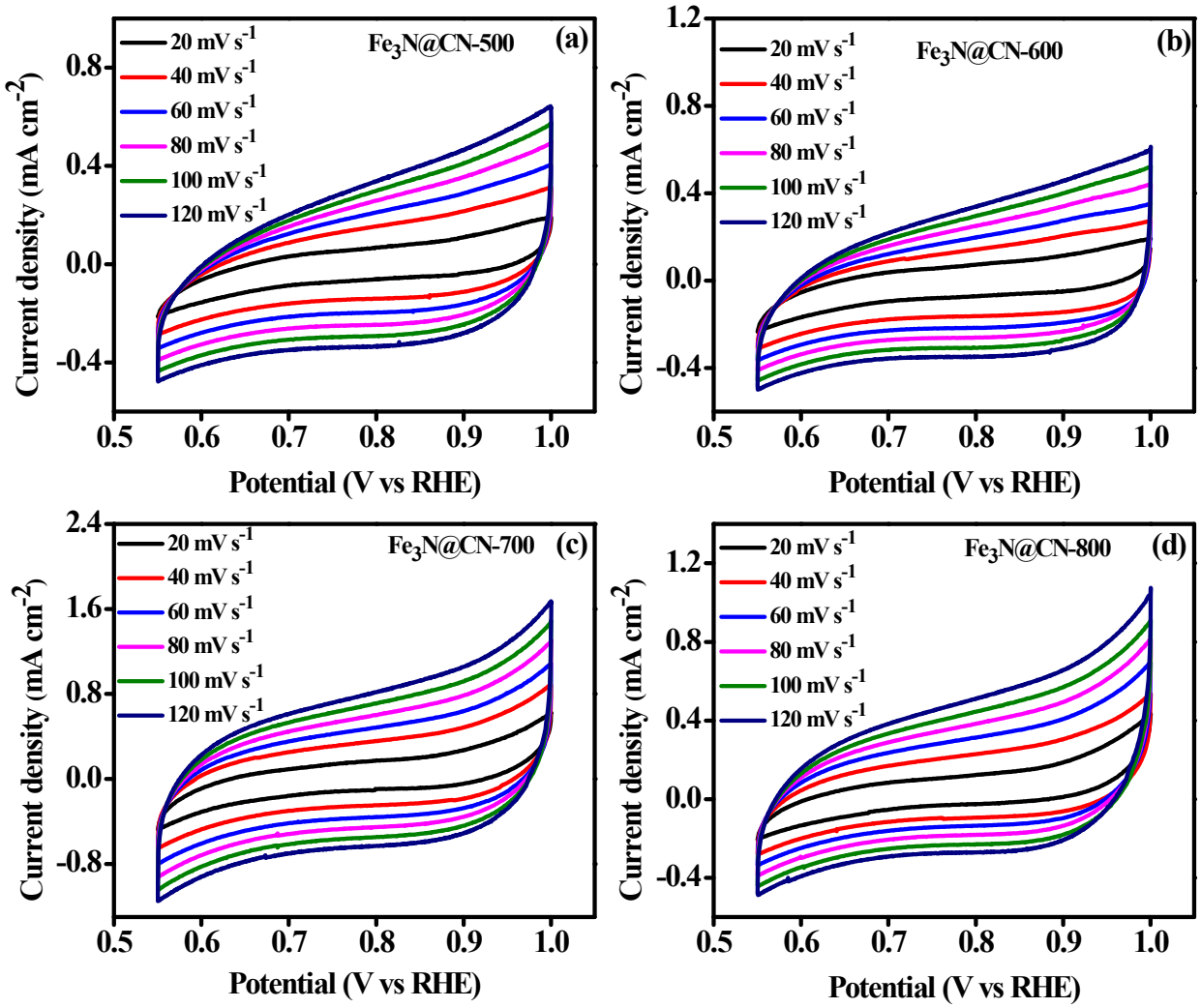

Figure S10. Faradaic efficiency of Fe_3N@CN-700 at applied current cell potential 1.64 V in 1.0 M KOH.

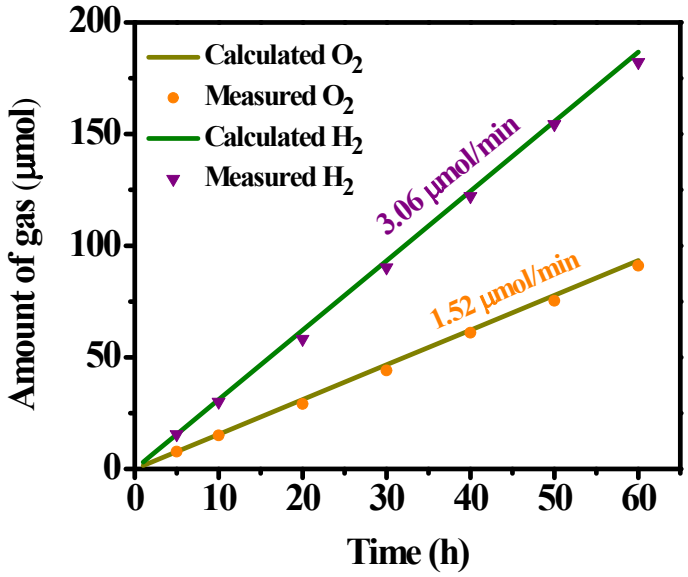

Figure S11. Post-XPS spectra of Fe_3N@CN-700 after 170 h of electrolysis; Fe 2p (a), O 1s (b) and N 1s (c)

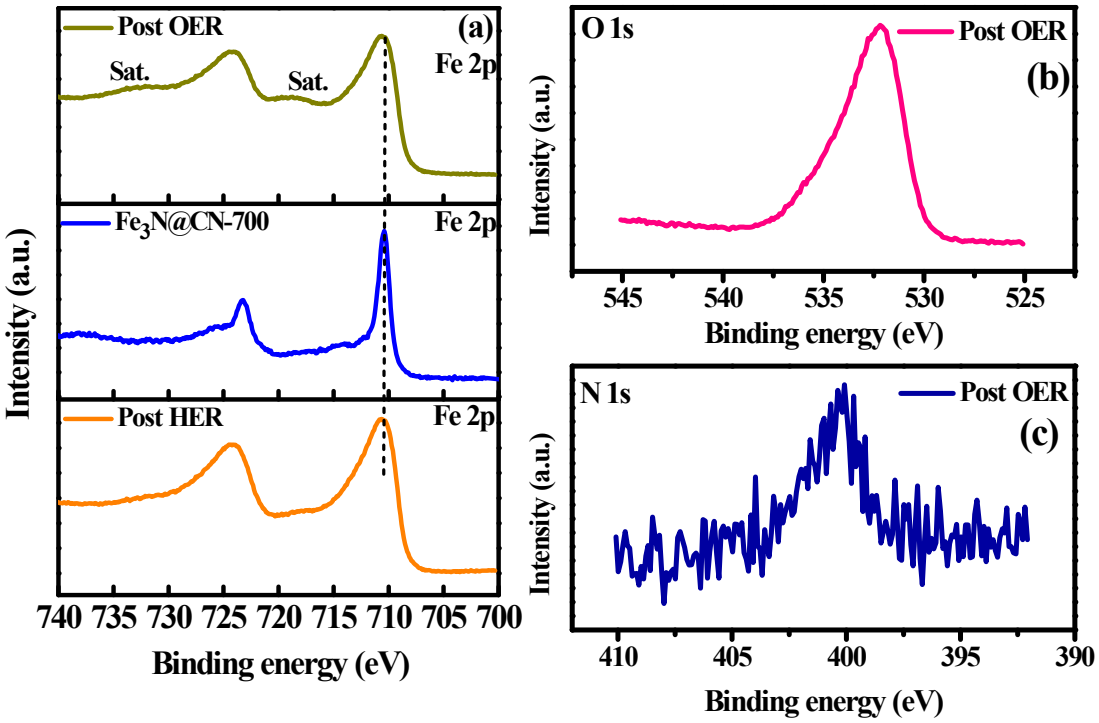

Table S1. Surface area, average pore size and pore volume of Fe_3N@CN-x

Catalyst	BET surface area (m^2/g)	Micropore Volume (cm^3/g) (Calculated from t-plot)	Pore Volume (cm^3/g) (Calculated from pores between 2.0 nm and 300 nm diameter by BJH method)	Average Pore Size (nm)
Fe_3N@CN-500	122.59	0.0418	0.105	3.45
Fe_3N@CN-600	126.03	0.0604	0.089	2.52
Fe_3N@CN-700	163.36	0.0600	0.141	3.22
Fe_3N@CN-800	148.02	0.0586	0.098	2.86

Table S2. Double layer capacitance and ECSA values of Fe_3N@CN-x

Catalyst	Double layer capacitance (mF cm^{-2})	ECSA (cm^2)
Fe_3N@CN-500	**2.2**	**55.0**
Fe_3N@CN-600	**2.3**	**57.5**
Fe_3N@CN-700	**5.6**	**140.0**
Fe_3N@CN-800	**2.7**	**67.5**

Table S3. Overall water electrolysis Fe-based electrocatalysts comparison in 1.0 M KOH electrolyte.

Catalyst	Catalyst support	Overall cell potential (V) @ 10 mA cm^{-2}	Durability (hour)	Reference
Fe_3N@CN-700	Nickel foam	1.64	170	This work
$Fe_{0.27}Co_{0.73}P$	Nickel foam	1.68	35	[9]
Co-Fe(1/1)-Se	Carbon cloth	1.68	9	[10]
Fe0.4Co0.6||Fe0.45Co0.55	CFPs	1.68	10	[11]
Ni-Fe-P-350	Nickel foam	1.67	40	[12]
EG/$Co_{0.85}$Se/ NiFe-LDH	EG foil	1.67	10 (20 mA cm^{-2})	[13]
(γ-FeOOH)/Ni_3S_2	Nickel foam	1.66	120	[14]
$Fe_{0.25}Co_{0.75}$	Carbon cloth	1.66	100	[15]
MoO_x-FeCoCu	Nickel foam	1.69	-	[16]
NiCoFeB nanochains	CFP	1.81	20	[17]
NiFeP-rGO//NiFeP-rGO	Nickel foam	1.66	45	[18]

Reference

1 J. Masa, S. Barwe, C. Andronescu, I. Sinev, A. Ruff, K. Jayaramulu, K. Elumeeva, B. Konkena, B. Roldan Cuenya and W. Schuhmann, *ACS Energy Lett.*, 2016, **1**, 1192–1198.

2 M. Liu, W. Zheng, S. Ran, S. T. Boles and L. Y. S. Lee, *Adv Materials Inter*, 2018, **5**, 1800849.

3 I. M. Mosa, S. Biswas, A. M. El-Sawy, V. Botu, C. Guild, W. Song, R. Ramprasad, J. F. Rusling and S. L. Suib, *Journal of Materials Chemistry A*, 2016, **4**, 620–631.

4 X. Hou, J. Li, J. Zheng, L. Li and W. Chu, *Dalton Transactions*, 2022, **51**, 13970–13977.

5 Y. Guo, T. Wang, J. Chen, J. Zheng, X. Li and K. (Ken) Ostrikov, *Advanced Energy Materials*, 2018, **8**, 1800085.

6 A. Forment-Aliaga, R. T. Weitz, A. S. Sagar, E. J. H. Lee, M. Konuma, M. Burghard and K. Kern, *Small*, 2008, **4**, 1671–1675.

7 A. N. Mansour, J. K. Ko, G. H. Waller, C. A. Martin, C. Zhang, X. Qiao, Y. Wang, X. Zhou and M. Balasubramanian, *ECS journal of solid state science and technology*, 2021, **10**, 103002.

8 X. He, L. Tian, M. Qiao, J. Zhang, W. Geng and Q. Zhang, *Journal of Materials Chemistry A*, 2019, **7**, 11478–11486.

9 C. Lin, P. Wang, H. Jin, J. Zhao, D. Chen, S. Liu, C. Zhang and S. Mu, *Dalton Transactions*, 2019, **48**, 16555–16561.

10 F. O. Boakye, Y. Li, K. A. Owusu, I. S. Amiinu, Y. Cheng and H. Zhang, *Materials Chemistry and Physics*, 2022, **275**, 125201.

11 W. Liu, K. Du, L. Liu, J. Zhang, Z. Zhu, Y. Shao and M. Li, *Nano Energy*, 2017, **38**, 576–584.

12 C. Xuan, J. Wang, W. Xia, Z. Peng, Z. Wu, W. Lei, K. Xia, H. L. Xin and D. Wang, *ACS Appl. Mater. Interfaces*, 2017, **9**, 26134–26142.

13 Y. Hou, M. R. Lohe, J. Zhang, S. Liu, X. Zhuang and X. Feng, *Energy & Environmental Science*, 2016, **9**, 478–483.

14 Y. Liu, M. Ding, Y. Tian, G. Zhao, J. Huang and X. Xu, *Journal of Colloid and Interface Science*, 2023, **639**, 24–32.

15 I. Walendzik, K. Kordek-Khalil and P. Rutkowski, *International Journal of Hydrogen Energy*.

16 J. Li, X. Gu, J. Chang, D. Wu, F. Xu, K. Jiang and Z. Gao, *Journal of Colloid and Interface Science*, 2022, **606**, 1662–1672.

17 Y. Li, B. Huang, Y. Sun, M. Luo, Y. Yang, Y. Qin, L. Wang, C. Li, F. Lv, W. Zhang and S. Guo, *Small*, 2019, **15**, 1804212.

18 J. Chang, Z. Hu, D. Wu, F. Xu, C. Chen, K. Jiang and Z. Gao, *Journal of Colloid and Interface Science*, 2023, **638**, 801–812.